

Journal Pre-proofs

Anti-inflammatory effects of an optimized PPAR- γ agonist *via* NF- κ B pathway inhibition

Zhiran Ju, Mingzhi Su, Jongki Hong, Eun La Kim, Jee H. Jung

PII: S0045-2068(19)31531-7
DOI: <https://doi.org/10.1016/j.bioorg.2020.103611>
Reference: YBIOO 103611

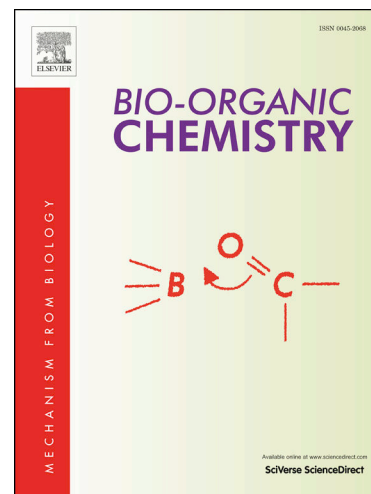
To appear in: *Bioorganic Chemistry*

Received Date: 15 September 2019
Revised Date: 14 January 2020
Accepted Date: 20 January 2020

Please cite this article as: Z. Ju, M. Su, J. Hong, E. La Kim, J.H. Jung, Anti-inflammatory effects of an optimized PPAR- γ agonist *via* NF- κ B pathway inhibition, *Bioorganic Chemistry* (2020), doi: <https://doi.org/10.1016/j.bioorg.2020.103611>

This is a PDF file of an article that has undergone enhancements after acceptance, such as the addition of a cover page and metadata, and formatting for readability, but it is not yet the definitive version of record. This version will undergo additional copyediting, typesetting and review before it is published in its final form, but we are providing this version to give early visibility of the article. Please note that, during the production process, errors may be discovered which could affect the content, and all legal disclaimers that apply to the journal pertain.

© 2020 Elsevier Inc. All rights reserved.



Anti-inflammatory effects of an optimized PPAR- γ agonist *via* NF- κ B pathway inhibition

Zhiran Ju ^{a,†}, Mingzhi Su ^{a,†}, Jongki Hong ^b, Eun La Kim ^a, Jee H. Jung ^{a,*}

^a College of Pharmacy, Pusan National University, Busan 46241, Republic of Korea

^b College of Pharmacy, Kyunghee University, Seoul 02447, Republic of Korea

*Correspondence: jhjung@pusan.ac.kr (J.H.J.); +82-51-510-2803 (J.H.J.).

†These authors equally contributed to this work

Abstract: In our previous study, a PPAR- γ agonist (+)-(*R,E*)-**6a1** was elaborated as an anti-inflammatory lead. However, *in silico* analysis showed that (+)-(*R,E*)-**6a1** lacks key hydrogen bonding with Tyr⁴⁷³ of PPAR- γ LBD (ligand binding domain). To facilitate additional hydrogen bonding with Tyr⁴⁷³, a more polar head group was introduced to the structure of (+)-(*R,E*)-**6a1**, and we also attempted to synthesize enzymatically stable derivatives. Of the synthetic derivatives, compound (+)-(*R,E*)-**5f** showed highest PPAR- γ transcriptional activity and reasonable metabolic stability. Compound (+)-(*R,E*)-**5f** suppressed the expression of pro-inflammatory mediators such as inducible NO synthase (iNOS), cyclooxygenase-2 (COX-2), interleukin 6 (IL-6), and tumor necrosis factor- α (TNF- α). Reduction of nitric oxide (NO), and ROS was also observed. Compound (+)-(*R,E*)-**5f** was found to suppress the NF- κ B pathway by inhibiting phosphorylation of IKK (I κ B kinase), and this may lead to subsequent inhibition of I κ B α (inhibitor of NF- κ B α) phosphorylation and inhibition of NF- κ B activation. These results indicate that (+)-(*R,E*)-**5f** exerts anti-inflammatory activity *via* NF- κ B pathway inhibition, and may serve as a potential anti-inflammatory lead.

Keywords: PPAR- γ agonist, anti-inflammatory, NF- κ B pathway, cyclooxygenase-2

1. Introduction

Inflammation, the fundamental defense mechanism of the immune system, can protect against injuries caused by harmful stimuli such as pathogens and poisons. However, excessive

inflammation, especially chronic inflammation, can cause immune system abnormalities and ultimately, pathogenesis [1]. The nuclear factor- κ B (NF- κ B) pathway has long been considered a prototypical pro-inflammatory signaling pathway, largely based on NF- κ B activation in the expression of pro-inflammatory cytokines such as interleukin 6 (IL-6) and tumor necrosis factor α (TNF α), and its role in the expression of other pro-inflammatory genes including chemokines and adhesion molecules [2-4]. The NF- κ B pathway has long been considered a preferred target for the development of new anti-inflammatory drugs.

Peroxisome proliferator-activated receptor γ (PPAR- γ), which can be modulated by direct binding of endogenous 15-deoxy- $\Delta^{12,14}$ -prostaglandin J₂ (15d-PGJ₂), is a member of the nuclear receptor superfamily. 15d-PGJ₂ and its derivatives, which possess an α,β -unsaturated ketone moiety can covalently bind to the thiol group of a cysteine residue (Cys²⁸⁵) in the PPAR- γ LBD through Michael addition reaction, and this additional covalent bonding contribute to the activation of PPAR- γ [5,9]. Binding of synthetic or natural ligands to PPAR- γ sequentially leads to activation, nuclear translocation, and transcriptional activation to modulate glucose and lipid metabolism [6]. Further research revealed that PPAR- γ also works as a negative regulator of inflammation, especially in macrophages [7,8]. In our previous study, we designed an exocyclic eneone jasmonate derivative (+)-(R,E)-**6a1**, which displayed significant PPAR- γ transcriptional activity and subsequent anti-inflammatory activity *via* inhibition of the NF- κ B pathway in macrophages [9,10]. Typical PPAR- γ ligands such as rosiglitazone and 15d-PGJ₂ comprise three distinct partial structures including a polar head, linker, and hydrophobic tail (Figure 1) [10]. The polar head and hydrophobic tail play important roles in H-bonding and hydrophobic interaction, respectively, with the PPAR- γ LBD (ligand binding domain). Compound (+)-(R,E)-**6a1** also contained these partial structures and showed remarkable PPAR- γ transactivation; *in silico* analysis showed that (+)-(R,E)-**6a1** binds to PPAR- γ in a manner similar to rosiglitazone and 15d-PGJ₂ (Figure 5). However, the binding pose of (+)-(R,E)-**6a1** lacks the key hydrogen bonding with tyrosine-473 (Tyr⁴⁷³). Hydrogen bonding with Tyr⁴⁷³ is important for the stabilization and activation of PPAR- γ [9-12]. Therefore, it would be beneficial if a more polar head, as a hydrogen bond acceptor, is introduced to the structure of (+)-(R,E)-**6a1**. Moreover, the head group of (+)-

(*R,E*)-**6a1** may be labile to enzymatic hydrolysis in the biological system. An obvious decrease in PPAR- γ activity with the free acid form of a similar compound has been observed previously [9].

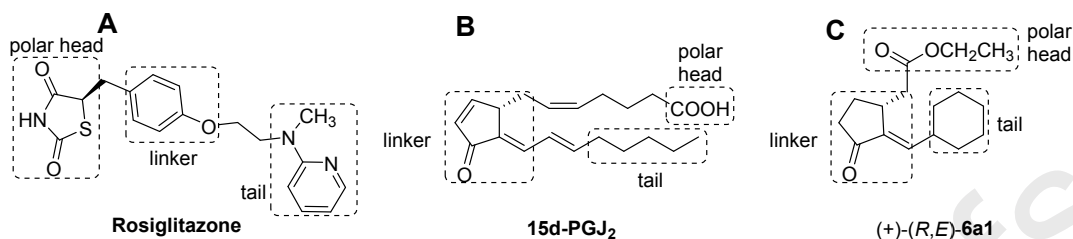


Figure 1. Structures and pharmacophoric regions of (A) rosiglitazone, (B) 15-deoxy- $\Delta^{12,14}$ prostaglandin J₂ (15d-PGJ₂), and (C) (+)-(*R,E*)-**6a1** [diagram from ref. 10]. Typical PPAR- γ agonists comprise a polar head and hydrophobic tail connected by a linker group.

In this study, to facilitate hydrogen bonding with Tyr⁴⁷³ and to improve metabolic stability, the head group of (+)-(*R,E*)-**6a1** was modified to various substituents (Figure 2), and evaluated for biological activity.

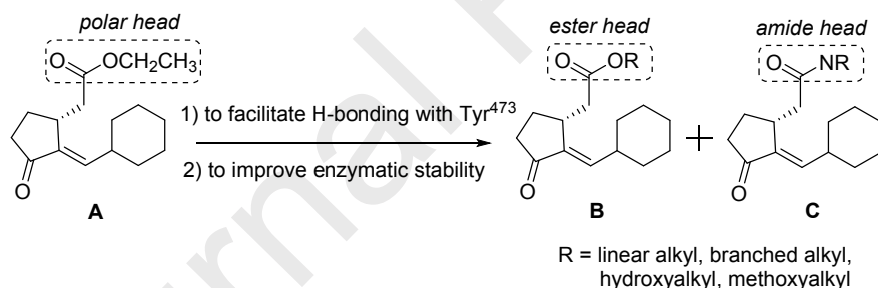


Figure 2. Design of (+)-(*R,E*)-**6a1** derivatives as PPAR- γ agonists with enhanced hydrogen bonding with Tyr⁴⁷³ and improved enzymatic stability. (A) (+)-(*R,E*)-**6a1**. (B) Designed analogs with an ester head. (C) Designed analogs with an amide head.

2. The strategy to design PPAR- γ activators based on (+)-(*R,E*)- **6a1**

Based on our original design, the polar head ethyl ester moiety was replaced with appropriately designed substituents that would facilitate additional hydrogen bonding with Tyr⁴⁷³ and/or resist enzymatic degradation in the biological system, retaining the desired potency of the parent molecule. To facilitate more hydrogen bonding with Tyr⁴⁷³, an

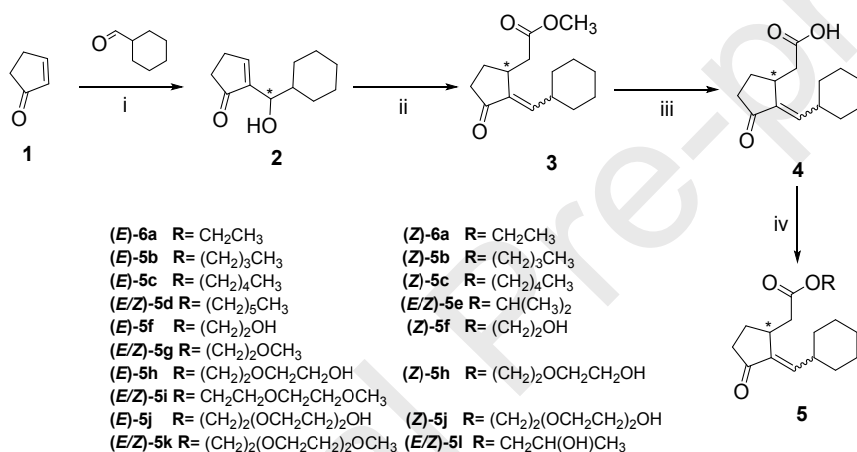
additional hydrogen bond acceptor such as hydroxyl, ether, or methoxyl group may be introduced. To improve metabolic stability, steric hindrance may be induced by introducing a long alkyl group, branched alkyl group, or other bulky groups that may suppress binding to hydrolytic enzymes. Based on this hypothesis, the metabolically labile ethyl ester moiety of (+)-(R,E)-**6a1** was replaced with linear alkyl, branched alkyl, hydroxyalkyl, or methoxyalkyl esters and amide derivatives (Schemes 1 and 2).

3. Results and discussion

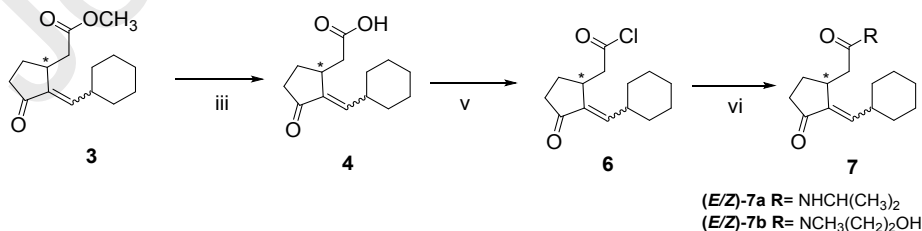
3.1. Chemistry

The synthetic routes of exocyclic enone derivatives are outlined in Schemes 1-3. The endocyclic ketones **2** were prepared from cyclopent-2-en-1-one **1** via a Baylis-Hillman reaction. Subsequent orthoester Claisen rearrangement [with MeC(OMe)₃ and propionic acid at 110°C] gave the exocyclic ketone **3** as a mixture of (*E*)/(*Z*) geometric isomers and inseparable *R/S* racemates of each geometric isomer with a yield of 80% (Scheme 1) [9,13,14]. Hydrolysis of **3** by LiOH in aqueous THF yielded the corresponding acid **4** (Scheme 1), which was further coupled with various alcohols in EtOAc using the coupling agent 2-(1H-benzotriazole-1-yl)-1,2,3,3-tetramethyluronium tetrafluoroborate (TBTU) to generate esters **6a**, **5b-5l** as mixtures of geometric and enantiomeric isomers. Compounds **7a-7b** were synthesized from **3** via three steps. The reactive acyl chloride **6** was prepared by treatment of acid **4** with oxalyl chloride in dichloromethane. The final amides **7a-7b** were consequently obtained as mixtures of geometric and enantiomeric isomers by coupling the acyl chloride **6** with isopropylamine or *N*-methylethanolamine, respectively, in the presence of *N,N'*-Dicyclohexylcarbodiimide (DCC), 1-hydroxybenzotriazole (HOBT), and triethylamine (TEA) in dichloromethane (Scheme 2) [15,16]. The (*E*) and (*Z*) isomers were interconvertible by a deconjugation/conjugation process under acidic reaction conditions. However, the thermodynamically more stable (*E*) isomer was the predominant product in most reactions (Table 1) [9]. The esters **6a**, **5b-5l**, and amides **7a-7b** were initially obtained as mixtures with various (*E*)/(*Z*) ratios, and the (*E*) or (*Z*) isomers can be separated by HPLC in a reasonably stable state in most cases, with the exception of other unstable isomers [9,17-19].

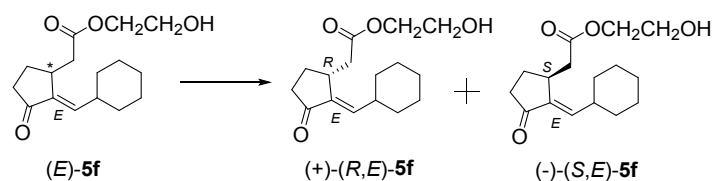
The geometric configurations of (*E*) and (*Z*) were determined by comparing the ^1H and ^{13}C -NMR data with the reported data of methyl (*2E*)-3-oxo-2-pentylidenecyclopentaneacetate [13]. In order to investigate the relative biological activity of each enantiomer of the most potent derivative of (*E*)-**5f** (Figure 3), the racemate of (*E*)-**5f** was further resolved into each enantiomer by chiral separation using a chiral cellulose column (Scheme 3). Each enantiomer was defined as (+)-(*R,E*)-**5f** ($[\alpha]_{\text{D}}^{20} = +5.5$, $c = 0.02$, CHCl_3) and (-)-(*S,E*)-**5f** ($[\alpha]_{\text{D}}^{20} = -6.0$, $c = 0.02$, CHCl_3) by comparing their specific rotations with those reported for similar compounds: methyl (+)-(*R,E*)-3-oxo-2-pentylidenecyclopentaneacetate ($[\alpha]_{\text{D}}^{20} = +21.3$, $c = 1.0$, CHCl_3) and methyl (-)-(*S,Z*)-3-oxo-2-pentylidenecyclopentan acetate ($[\alpha]_{\text{D}}^{20} = -1.4$, $c = 1.0$, CHCl_3).



Scheme 1: Reagents and conditions: i) Aldehyde, Bu_3P , BINOL, THF, N_2 , rt, 15 h; ii) MeC(OMe)_3 , propionic acid, 110°C , 15 h; iii) LiOH , THF-Water (3:2), rt, 12 h; iv) ROH, TBTU, TEA, EtOAc, rt, 12 h;



Scheme 2: Reagents and conditions: iii) LiOH , THF-Water (3:2), rt, 12 h; v) oxalyl chloride, CH_2Cl_2 , 40°C , 1 h; vi) RNH_2 , DDC, HOBT, TEA, CH_2Cl_2 , 40°C , 24 h.



Scheme 3: Conditions: Shimadzu LC-20A HPLC with a YMC chiral cellulose-C column, 22% Acetonitrile, flow rate: 1 ml/min, UV: 210, 254 nm. Retention time: (+)-(R,E)-**5f** at 180 min; (-)-(S,E)-**5f** at 190 min (*R*:*S* = 1:1).

3.2. PPAR- γ transactivation assay

The synthetic derivatives **6a**, **5b-5l**, and **7a-7b** were first screened for their *in vitro* PPAR- γ transactivation potency using Ac2F rat liver cells. Prior to the PPAR- γ transactivation assay, these derivatives were determined for their cytotoxicity to Ac2F cells to gauge the suitable concentration for performing the PPAR- γ transactivation assay. At concentrations of 5 and 10 μ M, these derivatives were mostly non-toxic to Ac2F cells, but **5l**, **7a**, and **7b** showed mild cytotoxicity in the tested cell lines (See SI). Therefore, the concentrations of 5 and 10 μ M were employed for the PPAR- γ transactivation assay. PPAR- γ agonistic activity was measured using Ac2F cells that had been transiently transfected with pcDNA3/pFlag-PPAR- γ 1 and PPRE. As shown in Figure 3, the differential activities of derivatives indicated that their PPAR- γ agonistic activity could be modulated by differential substitution at the carboxyl polar head group. Of these derivatives, the (*E*)-isomers frequently showed higher PPAR- γ transcriptional activity than (*Z*)-isomers as in the cases of (*E*)-**6a**, (*E*)-**5b**, (*E*)-**5c**, (*E*)-**5f**, and (*E*)-**5h**. This result was identical to that of our previous study [9], i.e., the *trans*-isomer was more active than the *cis*-isomer. The collected data also indicated that it is beneficial to introduce a hydroxyl group rather than a methoxyl group as shown by the significant activities of (*E*)-**5f**, (*E*)-**5h**, and (*E*)/(*Z*)-**5l**. Compound (*E*)-**5f** showed stronger PPAR- γ activation than rosiglitazone at the concentrations of 10 μ M, and its potency was enhanced compared to the original compound **6a1**. Despite improved metabolic stability (Table 1), the amide derivatives (*E*)/(*Z*)-**7a** and **-7b** showed decreased PPAR- γ agonistic

activity compared to **6a1**, possibly due to higher cytotoxicity than other compounds (see SI).

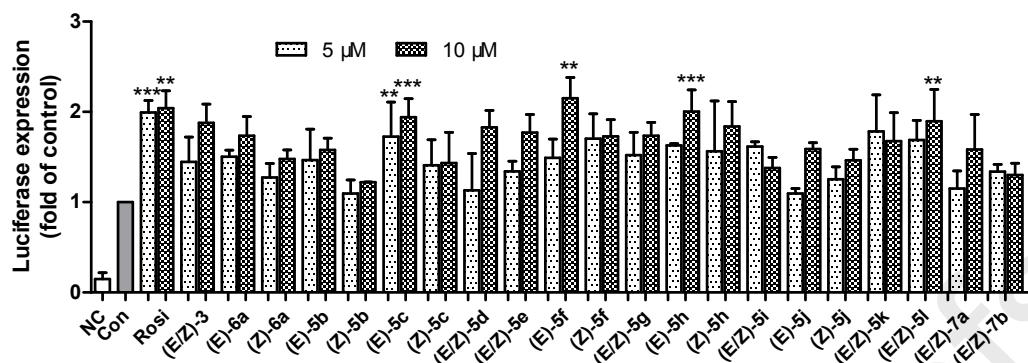


Figure 3. *In vitro* assay of PPAR- γ activation by compounds **3**, **6a**, **5b-5l**, **7a**, **7b**, and by rosiglitazone at 5 μ M or 10 μ M in rat liver Ac2F cells. NC: negative control, transfected with a plasmid containing PPRE and pcDNA3. Con: control, transfected with a plasmid containing PPRE and pFlag-PPAR- γ 1. Rosi: rosiglitazone. Rosiglitazone was used as the positive reference control to monitor activation of the luciferase reporter. Compound-treated cells were transiently transfected with PPRE plus pFlag-PPAR- γ 1. Luciferase expression (folds of the control) is presented as the mean \pm SD ($n = 3$). ** $p < 0.01$, *** $p < 0.001$.

The most potent derivative, (*E*)-**5f**, was further resolved into each enantiomer, (+)-(*R,E*)-**5f** and (-)-(*S,E*)-**5f**. The isomer (+)-(*R,E*)-**5f** showed almost equal activity to (-)-(*S,E*)-**5f** (Figure 4). Docking simulation suggested a higher binding affinity of (+)-(*R,E*)-**5f** (-8.2 Kcal/mol) than (-)-(*S,E*)-**5f** (-7.4 Kcal/mol) (Figure 6).

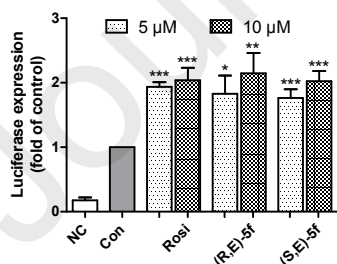


Figure 4. *In vitro* assay of PPAR- γ activation by (+)-(*R,E*)-**5f**, (-)-(*S,E*)-**5f** and by rosiglitazone at 5 μ M or 10 μ M in rat liver Ac2F cells. NC: negative control, transfected with a plasmid containing PPRE and pcDNA3. Con: control, transfected with a plasmid containing PPRE and pFlag-PPAR- γ 1. Rosi: rosiglitazone. Rosiglitazone was used as the positive

reference control to monitor activation of the luciferase reporter. Compound-treated cells were transiently transfected with PPRE plus pFlag-PPAR- γ 1. Luciferase expression (folds of the control) is presented as the mean \pm SD ($n = 3$). * $p < 0.05$, ** $p < 0.01$, *** $p < 0.001$.

The PPAR- γ agonistic potency of (+)-(R,E)-**5f** was further compared with rosiglitazone and 15dPGJ₂ at low concentrations (10 – 100 nM) (Figure 5). However, compound (+)-(R,E)-**5f** did not show higher potency than rosiglitazone and 15dPGJ₂ at lower concentrations.

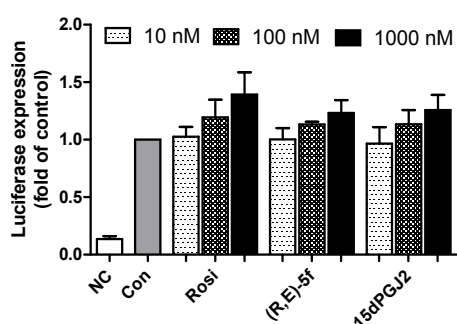


Figure 5. *In vitro* assay of PPAR- γ activation by (+)-(R,E)-**5f**, rosiglitazone, and 15dPGJ₂ at 10, 100, and 1000 nM in rat liver Ac2F cells. NC: negative control, transfected with a plasmid containing PPRE and pcDNA3. Con: control, transfected with a plasmid containing PPRE and pFlag-PPAR- γ 1. Compound-treated cells were transiently transfected with PPRE plus pFlag-PPAR- γ 1. Luciferase expression (folds of the control) is presented as the mean \pm SD ($n = 3$). * $p < 0.05$, ** $p < 0.01$, *** $p < 0.001$.

3.3. *In vitro* metabolic stability assay

The synthesized esters **3**, **6a**, **5b-5l**, and amides **7a-7b** were evaluated for *in vitro* metabolic stability using porcine liver esterase (PLE). The compounds were subjected to hydrolysis by incubating with PLE under special physiological conditions (phosphate buffer, pH 7.4, and 37°C) [15]. After 30 min and 60 min incubation, the reaction product was collected and analyzed by RP-HPLC to quantify the amount of the intact ester/amide and its corresponding metabolite (acid). The *in vitro* metabolic stability (ratio of esters/acids, amides/acids), and calculated log P value were employed as criteria for further lead selection (Table 1).

As shown in Table 1, the *in vitro* metabolic stability seems to be substantially modulated by polarity and steric hindrance of the ester/amide moiety. The linear alkyl esters **3**, **6a**, and **5b-5d** with a rather lipophilic property were highly susceptible to enzymatic hydrolysis, and the original peaks of esters were mostly replaced by peaks of their corresponding acids at 30 min and 60 min incubation with PLE. These results also suggested that extension of the linear alkyl chain is detrimental to their enzymatic stability. In contrast, branched ester **5e** was much more stable than linear alkyl esters **3**, **6a**, and **5b-5d**, even though it has similar lipophilicity. Further, the metabolic stability of the hydroxyl alkyl esters (**5f**, **5h**, **5j**, and **5l**) and the methoxyl alkyl esters (**5g**, **5i**, and **5k**) was significantly improved. In particular, significant improvement of metabolic stability was observed in hydroxyl alkyl esters **5f**, **5h**, **5j**, and **5l**, suggesting that resistance to enzymatic hydrolysis increases with increasing hydrophilicity. In addition, amides **7a-7b** showed stronger enzymatic stability compared to linear alkyl esters, and **7b** displayed the highest metabolic stability indicating that the amide bond is more resistant to enzymatic degradation. All these results suggest that branched alkyl esters or amides are more resistant to enzymatic hydrolysis than linear alkyl ones, and that hydrophilicity is an important factor for metabolic stability.

According to the collected results, (+)-(*R,E*)-**5f** was the most potent for PPAR- γ transactivation without notable cytotoxicity in normal cell lines and showed reasonably high enzymatic stability. Therefore, compound **5f** was selected for further biological evaluation.

Table 1. *In vitro* metabolic stability and (*E:Z*) ratio of synthetic derivatives

Compound.	Ratio (<i>E:Z</i>)	Log <i>P</i>	Stability	
			30 min	60 min
(<i>E</i>)- 6a / <i>(Z)</i> - 6a	15:1	3.20	0	0
(<i>E/Z</i>)- 3	NT	2.83	0	0
(<i>E</i>)- 5b / <i>(Z)</i> - 5b	33:1	4.26	0	0
(<i>E</i>)- 5c / <i>(Z)</i> - 5c	5:1	4.77	0	0
(<i>E/Z</i>)- 5d	8:1	5.27	0	0
(<i>E/Z</i>)- 5e	6:1	3.56	0.51±0.05	0
(<i>E</i>)- 5f / <i>(Z)</i> - 5f	4:1	2.10	2.21±0.31	1.40±0.25
(<i>E/Z</i>)- 5g	4:1	2.62	0.27±0.14	0
(<i>E</i>)- 5h / <i>(Z)</i> - 5h	8:1	1.90	1.71±0.25	0.43±0.10
(<i>E/Z</i>)- 5i	9:1	2.42	0.04±0.01	0
(<i>E</i>)- 5j / <i>(Z)</i> - 5j	7:1	1.69	1.02±0.16	0.33±0.07

(<i>E/Z</i>)- 5k	5:1	2.21	3.19±0.31	1.41±0.07
(<i>E/Z</i>)- 5l	7:1	2.56	4.28±0.42	1.77±0.20
(<i>E/Z</i>)- 7a	10:1	3.05	1.40±0.39	0.43±0.15
(<i>E/Z</i>)- 7b	6:1	1.99	17.50±0.34	2.88±0.40

Note: *In vitro* metabolic stability was determined by the esterase-catalyzed hydrolysis assay and was analyzed by HPLC. Data are presented as the ratio of intact esters (or amides) / hydrolyzed acids at 30 and 60 min, and are expressed as the mean ± SD (n=3) of three independent experiments; log *P* (octanol-water partition coefficient) values were calculated using Molinspiration software. For assessment of druglikeness of drug candidates, log *P* < 5 was considered a prerequisite for good bioavailability. NT: not tested.

3.4. Binding mode of (+)-(R,E)-**5f** to PPAR- γ

To gain insight into the interaction between compound (+)-(R,E)-**5f** and PPAR- γ , molecular docking simulation was performed using human PPAR- γ (PDB code: 2PRG) [20 - 22].

The best docking poses of compound (+)-(R,E)-**6a1**, (+)-(R,E)-**5f**, (+)-(R,Z)-**5f**, and (-)-(S,E)-**5f** are illustrated in Figure 6. Compound (+)-(R,E)-**6a1** formed hydrogen bonds with key amino acid residues, Ser²⁸⁹, His³²³, and Tyr³²⁷ on helices H3 and H4 in the PPAR- γ LBD (Figure 6A), but did not show direct hydrogen bonding with Tyr⁴⁷³ on the H12 helix. In contrast, compound (+)-(R,E)-**5f** showed hydrogen bonding with Tyr⁴⁷³ in addition to Tyr³²⁷, Ser²⁸⁹, Gln²⁸⁶, His³²³, and His⁴⁴⁹ on helices H3, H4, H11, and H12, in a similar pattern as rosiglitazone, but the affinity value was lower than that of rosiglitazone (-9.4 Kcal/mol) (Figure 6B). Additional interaction between (+)-(R,E)-**5f** and Tyr⁴⁷³ in the PPAR- γ LBD may lead to induction of H12 into the active conformation and thereby improve PPAR- γ transcriptional activity compared to (+)-(R,E)-**6a1**. It is reported that the Y473F mutant still retains the ability to bind covalently to 15d-PGJ₂, but loses the ligand-induced transcriptional activity [9,11,12]. Therefore, it is essential for a PPAR- γ agonist to form a hydrogen bond with Tyr⁴⁷³ for effective PPAR- γ activation. The geometric isomer (+)-(R,Z)-**5f** showed a similar binding pose as (+)-(R,E)-**5f**, but its affinity value (-7.4 Kcal/mol) was lower than that of (+)-(R,E)-**5f** (-8.2 Kcal/mol) (Figure 6C). Meanwhile, the enantiomer (-)-(S,E)-**5f** lost the

key interactions with amino acids Tyr³²⁷, Ser²⁸⁹, Gln²⁸⁶, His³²³, and Tyr⁴⁷³ (Figure 6D).

The docking calculation also showed that (+)-(*R,E*)-**5f** locates in the active cavity of PPAR- γ LBD in a similar manner as 15d-PGJ₂. Moreover, the thiol group of Cys²⁸⁵ is substantially close to the α,β -unsaturated enone group of (+)-(*R,E*)-**5f**, to facilitate a possible covalent agonism [11,12] (Figure 6B).

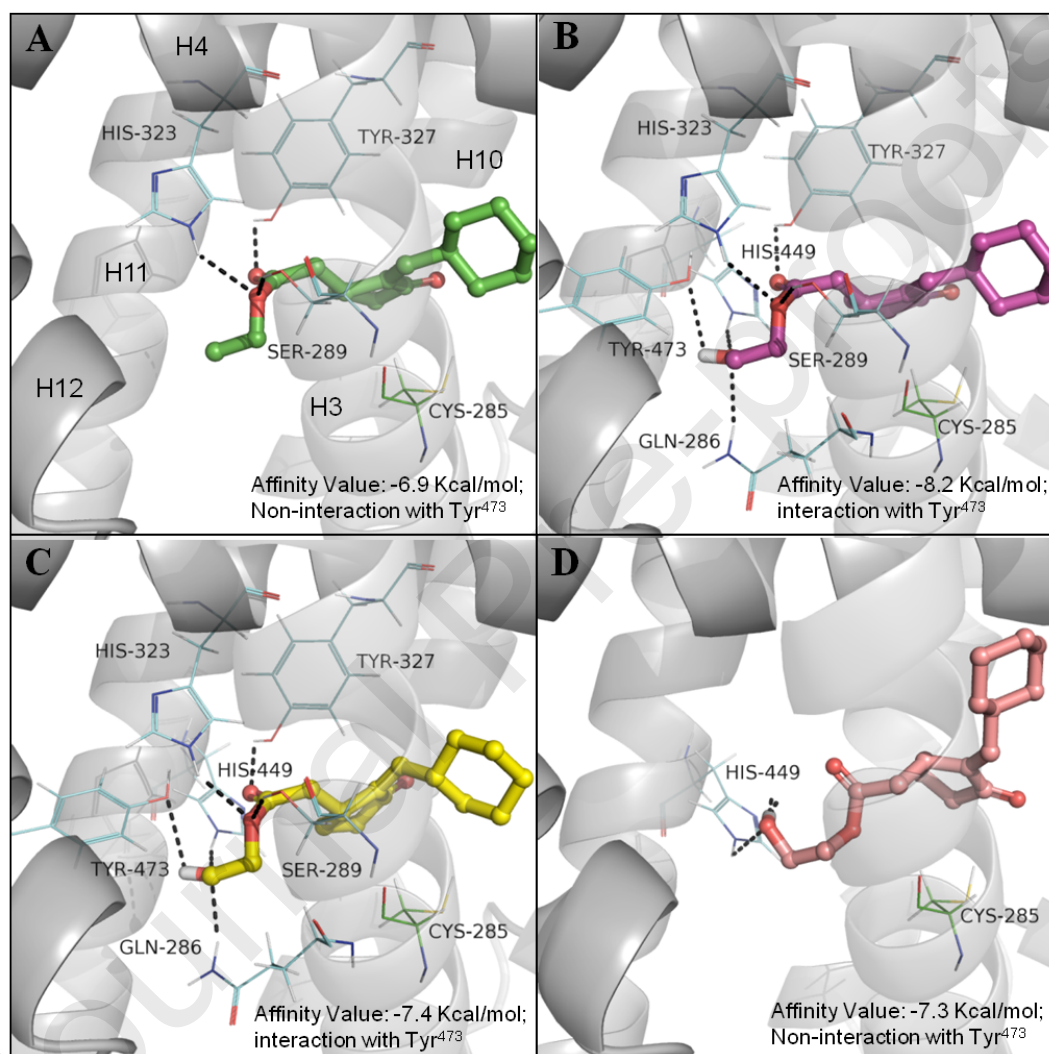


Figure 6. Docking structures of ligand/PPAR- γ binding. **(A)** Zoomed view of hydrogen bonding interactions (dotted lines) between the (+)-(*R,E*)-**6a1** and surrounding amino acids, Ser²⁸⁹, His³²³, and Tyr³²⁷. The key helices are labeled as H3, 4, 10, 11, and 12. **(B)** Zoomed view of hydrogen bonding interactions between (+)-(*R,E*)-**5f** and surrounding amino acids Tyr³²⁷, Ser²⁸⁹, Gln²⁸⁶, His³²³, His⁴⁴⁹, and Tyr⁴⁷³. **(C)** Zoomed view of hydrogen bonding interactions between (+)-(*R,Z*)-**5f** and surrounding amino acids Tyr³²⁷, Ser²⁸⁹, Gln²⁸⁶, His³²³, His⁴⁴⁹, and Tyr⁴⁷³. **(D)** Zoomed view of hydrogen bonding interactions between (-)-(*S,E*)-**5f**

and surrounding amino acid, His⁴⁴⁹.

3.5. (+)-(R,E)-**5f** inhibited LPS-induced expression of pro-inflammatory factors in RAW264.7 cells

Prior to the *in vitro* anti-inflammatory assay, the cytotoxicity of (+)-(R,E)-**5f** to murine macrophages (RAW 264.7) was first determined to gauge the suitable concentration for cell-based anti-inflammatory assays. The result indicated that (+)-(R,E)-**5f** showed no significant toxicity to RAW 264.7 cells at concentrations of 10 and 50 μ M for 24 h (See SI). Therefore, a concentration lower than 30 μ M for (+)-(R,E)-**5f** was applied to RAW 264.7 cells for the anti-inflammatory assay.

Some studies have reported that PPAR- γ protein can be expressed in macrophages, and that activated PPAR- γ translocates to the nucleus and binds NF- κ B. Binding with PPAR- γ leads to NF- κ B inhibition, thereby inhibiting the transcription of pro-inflammatory mediators such as iNOS, COX, TNF- α , and IL-6 [23]. Here, we used western blot analysis to assess the protein level of PPAR- γ translocated to the nucleus through activation by (+)-(R,E)-**5f**. As expected, the nuclear PPAR- γ protein level was significantly and concentration-dependently increased by (+)-(R,E)-**5f** treatment, and its potency was comparable to that of rosiglitazone at a concentration of 30 μ M (Figure 7).

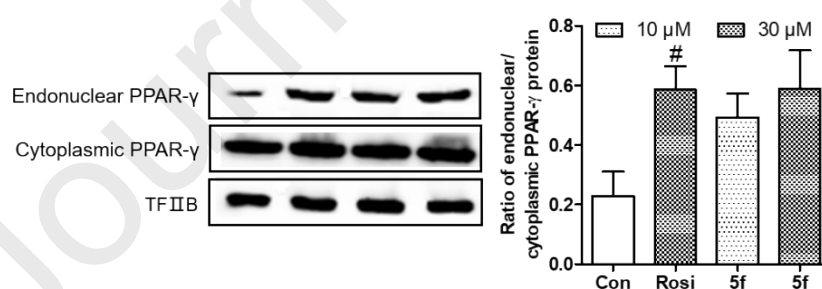


Figure 7. Endonuclear and cytoplasmic PPAR- γ protein levels in RAW264.7 macrophages treated with (+)-(R,E)-**5f** for 24 h as determined by western blotting. Nuclear levels of transcription Factor II B (TF II B) were used for reference purposes. The ratio of Nuclear/cytoplasmic PPAR- γ protein levels were shown as bar graph. Rosi: rosiglitazone. The results shown are representative of three independent experiments. [#] $p < 0.05$ compared with the control group.

At a very early stage of inflammation, macrophages are recruited to the inflammatory site and produce a large amount of pro-inflammatory molecules. For instance, nitric oxide (NO) and prostaglandin E₂ (PGE₂) are among these molecules, with a role in promoting the inflammation process [24]. Therefore, in order to investigate the anti-inflammatory activity of (+)-(R,E)-**5f**, the protein levels of pro-inflammatory factors iNOS and COX-2 were examined by western blot, employing RAW 264.7 cells. As shown in Figures 8A and 8B, LPS stimulation markedly increased the iNOS and COX-2 protein levels, but this increase was diminished in a dose-dependent manner after treatment with (+)-(R,E)-**5f**. The potency of (+)-(R,E)-**5f** at 10 μ M was comparable to that of dexamethasone. We used dexamethasone as a positive control in evaluation of anti-inflammatory activity because it is clinically used anti-inflammatory drug. Meanwhile, suppression of iNOS by (+)-(R,E)-**5f** is considered to cause decreased NO production in macrophages. As shown in Figure 9A, compound (+)-(R,E)-**5f** significantly and concentration-dependently decreased NO production.

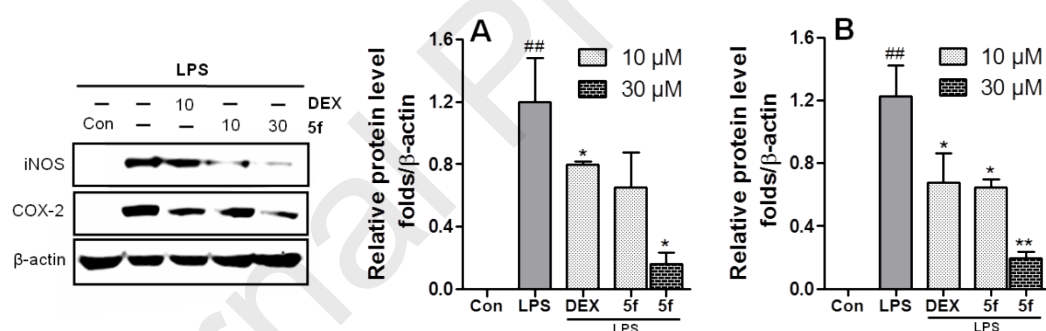


Figure 8. Effects of (+)-(R,E)-**5f** on LPS-induced iNOS (A) and COX-2 (B) protein expression in RAW264.7 cells. The cells were treated with different concentrations of (+)-(R,E)-**5f**, and then cultured in the presence or absence of LPS (1 μ g/ml) for 24 h. Dexamethasone (DEX) was employed as a positive control (10 μ M). The results are shown as the mean \pm SD (n = 3) of three independent experiments. $^{###}p < 0.01$ compared with the control group; $^*p < 0.05$, $^{**}p < 0.01$ compared with the LPS-stimulated group.

IL-6 and TNF- α are two cytokines that contribute to the progression of inflammation [25]. In acute and chronic inflammation, TNF- α is produced mainly by activated macrophages and plays a critical role in both tissue destruction and damage recovery, maintaining the

reversibility of inflammation. TNF- α may initiate an inflammatory cascade consisting of other inflammatory cytokines. Other studies have also indicated that TNF- α also acts as an inducer for nuclear factor- κ B (NF- κ B), which shows pro-inflammatory activity. So, inhibition of IL-6 and TNF- α production is effective strategy to suppress the progress of inflammation. The produced amounts of IL-6 and TNF- α were detected by enzyme-linked immunosorbent assay (ELISA). The results show that the amounts of IL-6 and TNF- α were markedly increased when murine macrophages RAW264.7 were exposed to LPS. However, these increases were inhibited by (+)-(R,E)-**5f** in a dose-dependent manner (Figures 9B and 9C), suggesting that (+)-(R,E)-**5f** as a PPAR- γ agonist could participate in a signaling pathway activated by LPS in macrophages [10,26,27].

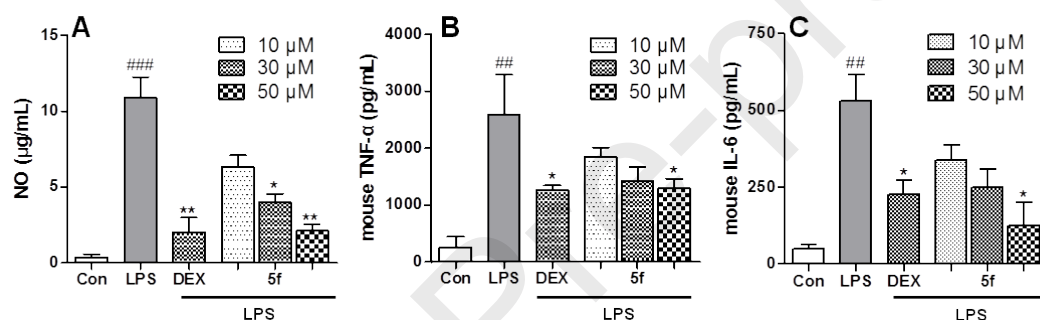


Figure 9. Inhibitory activity of (+)-(R,E)-**5f** on LPS-induced NO and cytokine production.

(A) The production of nitric oxide (NO) in the medium of RAW264.7 cells after treatment with (+)-(R,E)-**5f** for 1 h, and then with LPS (25 ng/mL, 24 h). The concentration of NO in the medium was determined using the Griess method. (B) Production of tumor necrosis factor α (TNF- α) in RAW264.7 cells after treatment with (+)-(R,E)-**5f** for 1 h, and then with LPS (25 ng/mL, 3 h). (C) Production of interleukin-6 (IL-6) in RAW264.7 cells after treatment with (+)-(R,E)-**5f** for 1 h, and then with LPS (25 ng/mL, 24 h). Dexamethasone was employed as a positive control (10 μ M). The results are shown as the mean \pm SD (n=3) of three independent experiments. ## $p < 0.01$, ### $p < 0.001$ compared with the control group; * $p < 0.05$, ** $p < 0.01$ compared with the LPS-stimulated group.

3.6. (+)-(R,E)-**5f** reduced ROS levels in RAW264.7 cells

In a biological system, reactive oxygen species (ROS), which include hydroxyl radical, superoxide anion, hydrogen peroxide, and singlet oxygen, play an important role in

inflammatory responses. COX-2 has also been implicated in ROS generation [28].

Overabundant ROS can oxidize and therefore damage endogenous molecules, which can lead to inflammation. ROS can activate redox-sensitive transcription factors such as NF- κ B and then influence pro-inflammatory responses. NF- κ B is involved in the regulation of pro-inflammatory genes, which represents a key step in the production of pro-inflammatory mediators such as TNF- α , IL-6, iNOS, and COX-2. Herein, we detected and quantified cellular oxidative stress. As shown in Figures 10A and 10B, compound (+)-(R,E)-**5f** dose-dependently reduced ROS production compared to the LPS-treatment group. Notably, at a concentration of 30 μ M, (+)-(R,E)-**5f** significantly decreased ROS production with a potency comparable to that of 10 μ M dexamethasone.

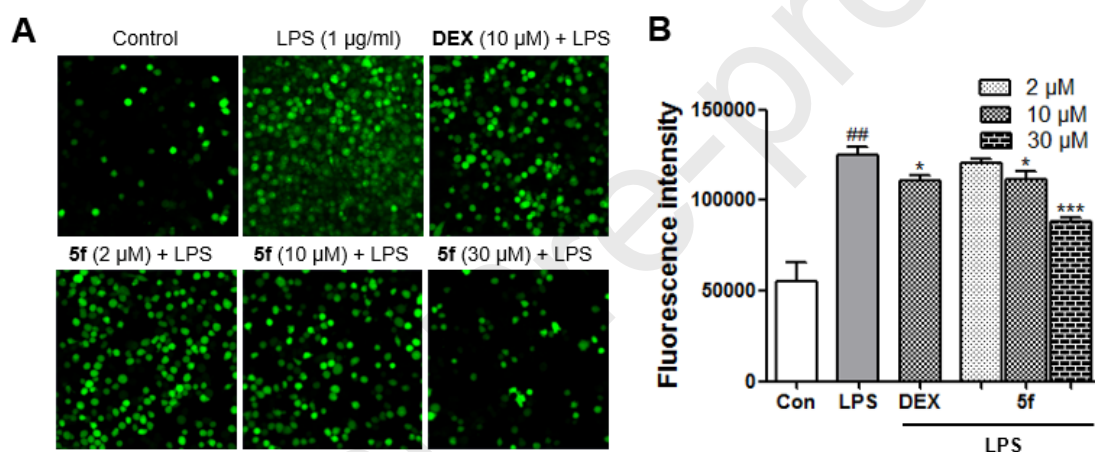


Figure 10. Reduction of ROS in RAW264.7 cells by treatment with (+)-(R,E)-**5f**. (A) LPS (1 μ g/mL) induced intracellular ROS, which is shown as green fluorescence using the fluorescent probe DCFH-DA. By treatment with (+)-(R,E)-**5f** or dexamethasone (DEX) (10 μ M), ROS expression was significantly decreased. (B) Fluorescence intensity was quantified using a fluorescence microplate reader. ## p < 0.01 vs untreated controls. * p < 0.05, *** p < 0.001 vs. LPS-treated cells.

3.7. (+)-(R,E)-**5f** inhibited LPS-induced NF- κ B signaling pathway in RAW264.7 cells

NF- κ B is a critical promoter involved in inflammation and in the induction of pro-inflammatory cytokines such as iNOS, COX-2, IL-6, and TNF- α . These cytokines play important roles in inflammation [29]. It has been recognized that conventional PPAR- γ ligands exert anti-inflammatory activity via binding to NF- κ B. Ligand-activated PPAR- γ may

be translocated into the nucleus to bind with NF- κ B. The NF- κ B/PPAR- γ complex cannot bind to the promoter region of DNA, leading to suppressed gene expression of pro-inflammatory mediators [10]. In an alternative pathway, PPAR- γ agonists such as 15d-PGJ₂ inhibit the NF- κ B activation pathway in the cytoplasm. In the cytoplasm, NF- κ B generally exists in an inactive NF- κ B-I κ B complex. Extracellular stimuli such as cytokines (i.e., TNF- α), pathogens, and endotoxin (i.e., lipopolysaccharides [LPS]) trigger the activation of IKK by phosphorylation. Activated IKK then phosphorylates I κ B with its subsequent ubiquitination and proteolytic degradation. After I κ B degradation, NF- κ B is released and translocates to the nucleus where it binds to the promoter regions of its target inflammatory genes. We intended to examine the effect of (+)-(R,E)-**5f** on the alternative pathway. As shown in Figure 11, the phosphorylation levels of NF- κ B increased significantly after LPS treatment, but the pre-treatment of (+)-(R,E)-**5f** obviously decreased the NF- κ B p65 phosphorylation in a dose-dependent manner (Figures 11A and 11B). As a result, the phosphorylated protein level of NF- κ B in the nucleus was also significantly decreased by (+)-(R,E)-**5f** treatment (Figure 11F). Meanwhile, the phosphorylation of IKK and I κ B α was decreased (Figures 11C and 11D) and I κ B α degradation was prevented in a dose-dependent manner (Figure 11E) by (+)-(R,E)-**5f** treatment. These results indicated that (+)-(R,E)-**5f** can inhibit the phosphorylation of IKK, and this may lead to subsequent inhibition of phosphorylation of I κ B α and NF- κ B.

To further investigate the downstream events of NF- κ B inhibition by (+)-(R,E)-**5f**, we examined the effect on the nuclear level of NF- κ B. In immunofluorescence assay, (+)-(R,E)-**5f** significantly reduced the nuclear level of phosphorylated NF- κ B (Figure 11G). Our findings suggest that (+)-(R,E)-**5f** may exert anti-inflammatory activity by inhibition of NF- κ B activation like PGJ₂ [10].

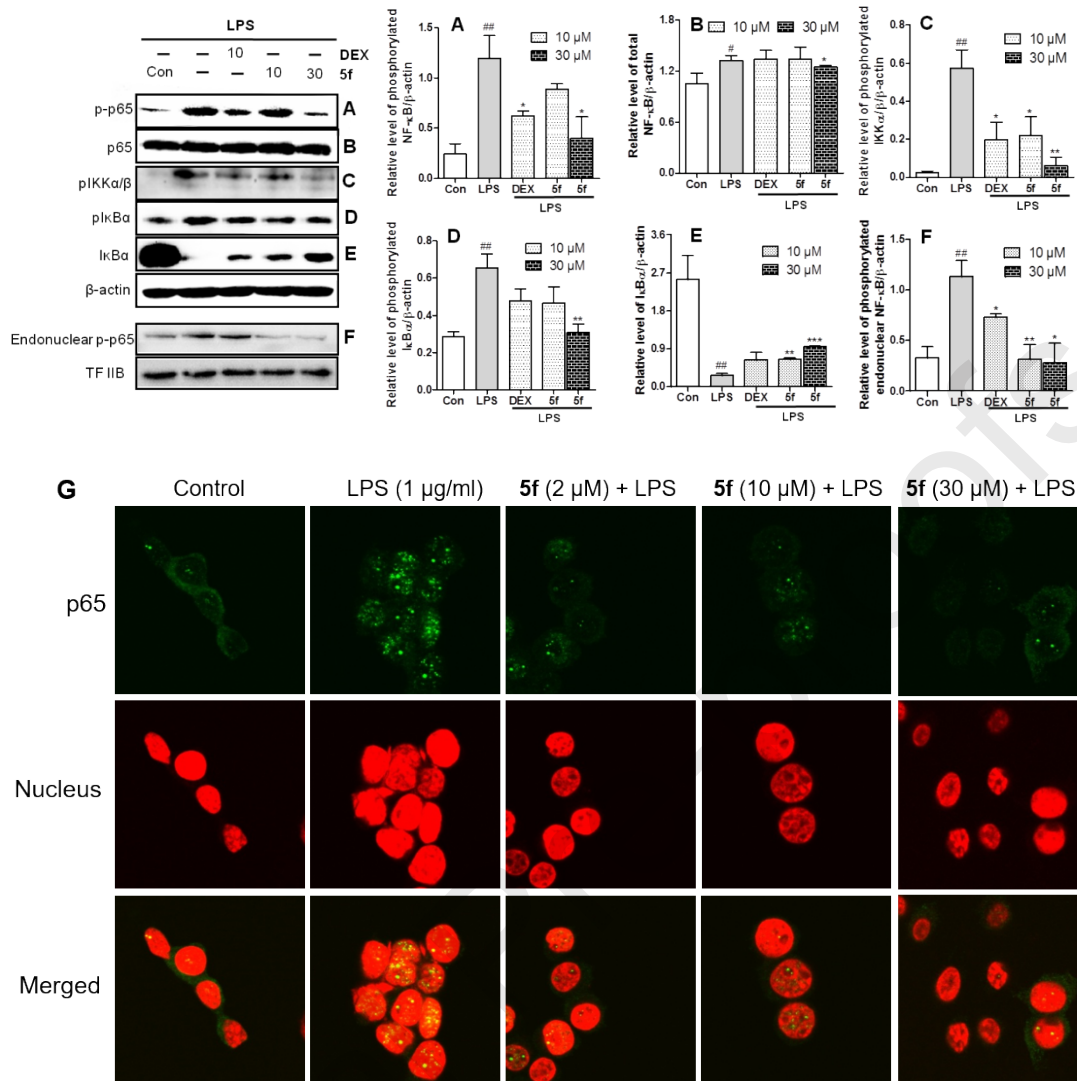


Figure 11. Inhibitory effect of (+)-(R,E)-5f on NF- κ B p65 activation in RAW 264.7 macrophages. (A) Phosphorylated NF- κ B p65 (total), (B) total NF- κ B p65, (C) phosphorylation of IKK, (D) phosphorylation of I κ B α , (E) intact I κ B α protein, and (F) phosphorylated nuclear NF- κ B p65 was determined by western blot. Cells were pretreated with (+)-(R,E)-5f for 1 h, and then stimulated with lipopolysaccharide (LPS, 25 ng/mL) for 30 min. β -actin was used as an internal control. (G) Immunofluorescence assay, NF- κ B p65 shows green fluorescence, and cell nuclei show red fluorescence by PI staining in confocal microscopy. The results shown are representative of three independent experiments. [#] $p < 0.05$, ^{##} $p < 0.01$ compared with the control group; ^{*} $p < 0.05$, ^{**} $p < 0.01$, ^{***} $p < 0.001$ compared with the LPS-stimulated group.

4. Conclusion

In this study, we designed and synthesized a series of potential PPAR- γ activators by further modifying the polar head of the previous lead (+)-(R,E)-**6a1**. The synthesized analogs were tested for their PPAR- γ transcriptional activity and *in vitro* metabolic stability. The differential PPAR- γ transcriptional activities of the geometric and enantiomeric isomers of selected compounds were also compared. The results indicated that (+)-(R,E)-**5f** might function as a potential PPAR- γ activator at the cellular level, and showed more potent PPAR- γ transcriptional activity and higher metabolic stability than (+)-(R,E)-**6a1**. Docking of (+)-(R,E)-**5f** to PPAR- γ showed that it locates in the active cavity of PPAR- γ LBD in a similar manner as rosiglitazone and 15d-PGJ₂. Moreover, the thiol group of Cys²⁸⁵ is substantially close to the α,β -unsaturated enone group of (+)-(R,E)-**5f**, to facilitate a possible covalent agonism like 15d-PGJ₂ [11,12]. *In vitro* anti-inflammatory assay indicated that (+)-(R,E)-**5f** exerted a significant anti-inflammatory activity through suppressed expression of pro-inflammatory factors including iNOS, COX-2, TNF- α , and IL-6 in LPS-stimulated murine RAW264.7 macrophages. Reduction of NO and ROS was also observed. The phosphorylation of IKK and I κ B α was decreased and I κ B α degradation was prevented in a dose-dependent manner by (+)-(R,E)-**5f** treatment. Treatment by (+)-(R,E)-**5f** obviously decreased the NF- κ B p65 phosphorylation and nuclear level of NF- κ B. Therefore, it is speculated that (+)-(R,E)-**5f** suppressed LPS-induced phosphorylation of IKK, leading to inhibition of I κ B α phosphorylation, and finally inhibition of NF- κ B activation. The upgraded PPAR- γ agonist (+)-(R,E)-**5f** is expected to serve as a lead for the study of potential anti-inflammatory agents.

5. Experimental section

5.1. Chemistry

All reagents used were commercially available; some organic solvents were redistilled under positive pressure if necessary. Reactions were monitored by thin-layer chromatography (TLC) on glass plates coated with silica gel using a fluorescent indicator (GF254). The ¹H- and ¹³C-NMR spectral data were recorded on Varian Unity 500 MHz and 400 MHz NMR spectrometer, respectively. High-resolution fast-atom bombardment mass spectrometry (HRFABMS) data were obtained using an Agilent 1200 UHPLC accurate-mass Q-TOF MS

spectrometer. The optical rotation data were obtained using a Jasco P-1020 Polarimeter.

HPLC analysis was performed on a YMC ODS-Triart C18 column (250 × 10 mm, 5 μm, 120 Å) and a YMC chiral cellulose-C column (250 × 10 mm, 5 μm, 100 Å) using a Shodex RI-71 detector and Shimadzu LC-20A HPLC. All chemical reagents were purchased from Sigma-Aldrich and Alfa Aesar.

5.1.1. Synthesis of compounds **6a**, **5b-5l**

General Procedure A: Baylis-Hillman reaction. A solution of cyclopent-2-en-1-one (1.0 mol-equiv.), the appropriate aldehyde (1.5 mol-equiv.), [1,1'-binaphthalene]-2,2'-diol (0.1 mol-equiv.), and Bu₃P (0.2 mol-equiv.) in THF (25 ml) was stirred at room temperature in the presence of N₂ for 15 h. *General Procedure B:* Orthoester Claisen rearrangement reaction. A reaction product from Baylis-Hillman reaction, trimethyl orthoacetate (6 ml), was heated with propionic acid (a few drops) at 110°C for 18 h. The crude mixture was evaporated, and the residue was subjected to HPLC (Shodex RI-71 Detector, 65% Methanol, flow rate: 2 ml/min) to separate the desired product **3**, from the apolar aldehyde, Bu₃P, and polar compound [1,1'-binaphthalene]-2,2'-diol. *General Procedure C:* Hydrolysis reaction. Lithium hydroxide (LiOH) (1N, 2 equiv) was added to a solution of compound **3** (1 equiv) in aqueous THF (THF: water = 3:2), and the reaction mixture was stirred at 40°C for 12 h. The THF was evaporated under vacuum and the water layer was neutralized with (1N, 2 equiv) HCl. The resulting suspension was extracted with EtOAc (three times). The combined organic layer was washed with brine, dried over MgSO₄, concentrated to yield the acid **4**, which was used without purification for the next step. 2-(1*H*-Benzotriazole-1-yl)-1,2,3,3-tetramethyluronium tetrafluoroborate (TBTU, 1 equiv) was added to a solution of compound **4** and triethylamine (TEA, 2 equiv) in EtOAc. After 10 min of stirring at room temperature, alcohols (2 equiv) were added separately and the reaction mixture was stirred for 12 h. The mixture was washed with water, dried, and concentrated to give a residue that was purified by reversed-phase HPLC (YMC ODS-Triart C18 column) to yield the target esters **6a-5l**.

5.1.2. Ethyl-2-(2-(cyclohexylmethylene)-3-oxocyclopentyl)acetate (*E*)-**6a**

Yellow oil; 45% yield; ¹H-NMR (500 MHz, CD₃OD) δ 6.40 (dd, *J* = 10.7, 1.9 Hz, 1H), 4.22

(q, $J = 7.1$ Hz, 2H), 3.50 (m, 1H), 2.57 (m, 2H), 2.50 (m, 1H), 2.34 (m, 2H), 2.11 (m, 1H), 1.95 (m, 1H), 1.83 (m, 2H), 1.70 (m, 2H), 1.44 (m, 2H), 1.20-1.36 (m, 4H), 1.33 (m, 3H), ^{13}C -NMR (125 MHz, CD_3OD) δ 209.0, 173.4, 143.6, 139.4, 61.6, 40.3, 39.5, 36.6, 36.2, 33.1, 33.0, 26.8, 26.4 ($\times 2$), 26.3, 14.5. HRFABMS m/z 265.1798 $[\text{M}+\text{H}]^+$ (calcd for $\text{C}_{16}\text{H}_{24}\text{O}_3$, 265.1798).

5.1.3. Ethyl-2-(2-(cyclohexylmethylene)-3-oxocyclopentyl)acetate (Z)-6a

Yellow oil; 3% yield; ^1H -NMR (500 MHz, CD_3OD) δ 5.82 (dd, $J = 9.6, 1.0$ Hz, 1H), 4.17 (q, $J = 7.1$ Hz, 2H), 3.45 (m, 1H), 2.63 (m, 1H), 2.43 (m, 1H), 2.35 (m, 1H), 2.28 (m, 1H), 2.19 (m, 1H), 2.06 (d, $J = 1.2$ Hz, 2H), 1.73 (m, 2H), 1.67 (m, 2H), 1.62 (m, 2H), 1.36 (m, 2H), 1.28 (m, 3H), 1.10 (m, 2H). ^{13}C -NMR (125 MHz, CD_3OD) δ 209.6, 173.8, 147.7, 137.8, 61.5, 40.4, 39.9, 39.0, 36.9, 33.7, 33.4, 27.5, 26.9, 26.6 ($\times 2$), 14.5. HRFABMS m/z 265.1798 $[\text{M}+\text{H}]^+$ (calcd for $\text{C}_{16}\text{H}_{24}\text{O}_3$, 265.1798).

5.1.4. Butyl-2-(2-(cyclohexylmethylene)-3-oxocyclopentyl)acetate (E)-5b

Yellow oil; 66% yield; ^1H -NMR (500 MHz, CD_3OD) δ 6.39 (dd, $J = 10.7, 1.6$ Hz, 1H), 4.14 (t, $J = 6.6$ Hz, 2H), 3.49 (m, 1H), 2.54 (m, 2H), 2.47 (m, 1H), 2.32 (m, 2H), 2.08 (m, 1H), 1.92 (m, 1H), 1.80 (m, 2H), 1.66 (m, 4H), 1.49-1.20 (m, 8H), 0.99 (t, $J = 7.4$ Hz, 3H). ^{13}C -NMR (125 MHz, CD_3OD) δ 209.1, 173.5, 143.6, 139.5, 65.5, 40.4, 39.6, 36.6, 36.3, 33.1, 33.0, 31.8, 26.8, 26.4, 26.4, 26.3, 20.2, 14.0. HRFABMS m/z 293.2112 $[\text{M}+\text{H}]^+$ (calcd for $\text{C}_{18}\text{H}_{28}\text{O}_3$, 293.2111).

5.1.5. Butyl-2-(2-(cyclohexylmethylene)-3-oxocyclopentyl)acetate (Z)-5b

Yellow oil; 2% yield; ^1H -NMR (500 MHz, CD_3OD) δ 5.80 (dd, $J = 9.6, 2.1$ Hz, 1H), 4.11 (t, $J = 6.6$ Hz, 2H), 3.45 (m, 1H), 2.61 (m, 2H), 2.43 (m, 1H), 2.31 (m, 1H), 2.19 (m, 1H), 1.63-1.51 (m, 6H), 1.39 (m, 6H), 1.22 (m, 2H), 1.08 (m, 2H), 0.96 (t, $J = 7.4$ Hz, 3H). ^{13}C -NMR (125 MHz, CD_3OD) δ 209.6, 173.8, 147.7, 137.9, 65.4, 40.4, 39.9, 39.0, 36.9, 33.7, 33.4, 31.8, 27.5, 27.0, 26.6 ($\times 2$), 20.2, 14.0. HRFABMS m/z 293.2112 $[\text{M}+\text{H}]^+$ (calcd for $\text{C}_{18}\text{H}_{28}\text{O}_3$, 293.2111).

5.1.6. Pentyl-2-(2-(cyclohexylmethylene)-3-oxocyclopentyl)acetate (E)-5c

Yellow oil; 50% yield; $^1\text{H-NMR}$ (500 MHz, CD_3OD) δ 6.38 (dd, $J = 10.4, 1.5$ Hz, 1H), 4.12 (t, $J = 6.7$ Hz, 2H), 3.49 (m, 1H), 2.56 (m, 2H), 2.46 (m, 1H) 2.31 (m, 2H), 2.07 (m, 1H), 1.92 (m, 1H), 1.76 (m, 2H), 1.67 (m, 4H), 1.39 (m, 6H), 1.26 (m, 4H), 0.95 (t, $J = 7.6$ Hz, 3H). $^{13}\text{C-NMR}$ (125 MHz, CD_3OD) δ 209.3, 173.6, 143.7, 139.5, 65.8, 40.5, 39.6, 36.6, 36.3, 33.1, 33.0, 29.4, 29.3, 26.8, 26.4 ($\times 2$), 26.3, 23.3, 14.3. HRFABMS m/z 307.2268 $[\text{M}+\text{H}]^+$ (calcd for $\text{C}_{19}\text{H}_{30}\text{O}_3$, 307.2268).

5.1.7. *Pentyl-2-(2-(cyclohexylmethylene)-3-oxocyclopentyl)acetate (Z)-5c*

Yellow oil; 10% yield; $^1\text{H-NMR}$ (500 MHz, CD_3OD) δ 5.81 (dd, $J = 9.6, 2.2$ Hz, 1H), 4.12 (t, $J = 6.7$ Hz, 2H), 3.46 (m, 1H), 2.60 (m, 2H), 2.50 (m, 1H) 2.31 (m, 2H), 2.18 (m, 1H), 1.92 (m, 1H), 1.77 (m, 2H), 1.66 (m, 4H), 1.35 (m, 6H), 1.25 (m, 2H), 1.09 (m, 2H), 0.95 (t, $J = 7.8$ Hz, 3H). $^{13}\text{C-NMR}$ (125 MHz, CD_3OD) δ 208.0, 172.6, 146.5, 136.7, 64.5, 39.1, 38.7, 37.8, 35.7, 32.5, 32.1, 28.2, 28.0, 26.3, 25.7, 25.4 ($\times 2$), 22.1, 13.0. HRFABMS m/z 307.2268 $[\text{M}+\text{H}]^+$ (calcd for $\text{C}_{19}\text{H}_{30}\text{O}_3$, 307.2268).

5.1.8. *Hexyl-2-(2-(cyclohexylmethylene)-3-oxocyclopentyl)acetate (E/Z)-5d*

Yellow oil; 60% yield; $^1\text{H-NMR}$ (500 MHz, CD_3OD) δ 6.38 (dd, $J = 10.6, 1.4$ Hz, 1H), 4.12 (t, $J = 6.4$ Hz, 2H), 3.49 (m, 1H), 2.54 (m, 2H), 2.45 (m, 1H) 2.31 (m, 2H), 2.06 (m, 1H), 1.90 (m, 1H), 1.79 (m, 2H), 1.65 (m, 4H), 1.39 (m, 8H), 1.26 (m, 4H), 0.94 (t, $J = 7.6$ Hz, 3H). $^{13}\text{C-NMR}$ (125 MHz, CD_3OD) δ 209.2, 173.6, 143.7, 139.5, 65.8, 40.5, 39.6, 36.6, 36.3, 33.1, 33.0, 32.5, 29.7, 26.8, 26.7, 26.4 ($\times 2$), 26.3, 23.6, 14.3. HRFABMS m/z 321.2424 $[\text{M}+\text{H}]^+$ (calcd for $\text{C}_{20}\text{H}_{32}\text{O}_3$, 321.242).

5.1.9. *Isopropyl-2-(2-(cyclohexylmethylene)-3-oxocyclopentyl)acetate (E/Z)-5e*

Yellow oil; 45% yield. $^1\text{H-NMR}$ (500 MHz, CD_3OD) δ 6.34 (dd, $J = 10.6, 1.9$ Hz, 1H), 4.98 (qd, $J = 12.6, 6.2$ Hz, 1H), 3.43 (m, 1H), 2.47 (m, 2H), 2.41 (m, 1H) 2.27 (m, 2H), 2.03 (m, 1H), 1.88 (m, 1H), 1.76 (m, 2H), 1.65 (m, 4H), 1.36 (m, 2H), 1.25 (d, $J = 3.1$ Hz, 3H), 1.23 (d, $J = 3.1$ Hz, 3H), 1.18 (m, 2H). $^{13}\text{C-NMR}$ (125 MHz, CD_3OD) δ 209.3, 173.1, 143.7, 139.5, 69.4, 40.7, 39.6, 36.7, 36.2, 33.1, 33.0, 26.8, 26.4, 26.3, 26.3, 22.1, 22.0. HRFABMS m/z 279.1955 $[\text{M}+\text{H}]^+$ (calcd for $\text{C}_{17}\text{H}_{26}\text{O}_3$, 279.1955).

5.1.10. 2-Hydroxyethyl-2-(2-(cyclohexylmethylene)-3-oxocyclopentyl)acetate (E)-5f

Yellow oil; 40% yield; ¹H-NMR (500 MHz, CD₃OD) δ 6.38 (dd, *J* = 10.7, 1.9 Hz, 1H), 4.20 (t, *J* = 6.7 Hz, 2H), 3.77 (t, *J* = 6.7 Hz, 2H), 3.47 (m, 1H), 2.67 (m, 1H), 2.46 (m, 1H), 2.33 (m, 2H), 2.21 (m, 1H), 1.66 (m, 8H), 1.73 (m, 6H), 1.25 (m, 5H). ¹³C-NMR (125 MHz, CD₃OD) δ 209.5, 173.6, 143.8, 139.5, 67.1, 60.9, 40.2, 39.6, 36.7, 36.2, 33.1, 33.0, 26.8, 26.4 (×2), 26.3. HRFABMS *m/z* 281.1746 [M+H]⁺ (calcd for C₁₆H₂₄O₄, 281.1747).

5.1.11. 2-Hydroxyethyl-2-(2-(cyclohexylmethylene)-3-oxocyclopentyl)acetate (Z)-5f

Yellow oil; 10% yield; ¹H-NMR (500 MHz, CD₃OD) δ 5.84 (dd, *J* = 9.6, 2.1 Hz, 1H), 4.18 (t, *J* = 6.8 Hz, 2H), 3.75 (t, *J* = 6.8 Hz, 2H), 3.45 (m, 1H), 2.67 (m, 1H), 2.46 (m, 2H), 2.33 (m, 2H), 2.21 (m, 1H), 1.66 (m, 8H), 1.35 (m, 1H), 1.25 (m, 2H), 1.11 (m, 1H). ¹³C-NMR (125 MHz, CD₃OD) δ 209.6, 173.8, 147.8, 137.8, 66.9, 60.9, 40.2, 39.9, 39.0, 36.9, 33.6, 33.3, 27.5, 27.0, 26.6 (×2). HRFABMS *m/z* 281.1746 [M+H]⁺ (calcd for C₁₆H₂₄O₄, 281.1747).

5.1.12. 2-Methoxyethyl-2-(2-(cyclohexylmethylene)-3-oxocyclopentyl)acetate (E/Z)-5g

Yellow oil; 50% yield; ¹H-NMR (500 MHz, CD₃OD) δ 6.39 (dd, *J* = 10.7, 1.9 Hz, 1H), 4.27 (t, *J* = 6.8 Hz, 2H), 3.64 (t, *J* = 6.6 Hz, 2H), 3.49 (m, 1H), 3.40 (s, 3H), 2.56 (m, 2H), 2.49 (m, 1H), 2.32 (m, 2H), 2.08 (m, 1H), 1.94 (m, 1H), 1.80 (m, 2H), 1.67 (m, 2H), 1.21-1.48 (m, 6H). ¹³C-NMR (125 MHz, CD₃OD) δ 209.3, 173.4, 143.8, 139.4, 71.4, 64.6, 59.0, 40.2, 39.6, 36.6, 36.2, 33.1, 33.0, 26.8, 26.4, 26.3, 26.3. HRFABMS *m/z* 295.1903 [M+H]⁺ (calcd for C₁₇H₂₆O₄, 295.1904).

5.1.13. 2-(2-Hydroxyethoxy)ethyl-2-(2-(cyclohexylmethylene)-3-oxocyclopentyl)acetate (E)-

5h

Yellow oil; 48% yield; ¹H-NMR (500 MHz, CD₃OD) δ 6.35 (dd, *J* = 10.7, 1.8 Hz, 1H), 4.24 (t, *J* = 6.8 Hz, 2H), 3.70 (t, *J* = 6.6 Hz, 2H), 3.66 (t, *J* = 6.6 Hz, 2H), 3.56 (t, *J* = 6.6 Hz, 2H), 3.45 (m, 1H), 2.53 (m, 2H), 2.45 (m, 1H), 2.30 (m, 2H), 2.04 (m, 1H), 1.90 (m, 1H), 1.75 (m, 2H), 1.63 (m, 2H), 1.19-1.48 (m, 6H). ¹³C-NMR (125 MHz, CD₃OD) δ 209.3, 173.4, 143.7, 139.5, 73.6, 70.0, 64.8, 62.1, 40.2, 39.6, 36.6, 36.2, 33.1, 33.0, 26.8, 26.4, 26.3 (×2). HRFABMS *m/z* 325.2011 [M+H]⁺ (calcd for C₁₈H₂₈O₅, 325.2010).

5.1.14. 2-(2-Hydroxyethoxy)ethyl-2-(2-(cyclohexylmethylene)-3-oxocyclopentyl)acetate (Z)-

5h

Yellow oil; 6% yield; ¹H-NMR (500 MHz, CD₃OD) δ 5.81 (dd, *J* = 9.6, 2.0 Hz, 1H), 4.24 (t, *J* = 6.8 Hz, 2H), 3.70 (t, *J* = 6.6 Hz, 2H), 3.65 (t, *J* = 6.6 Hz, 2H), 3.56 (t, *J* = 6.4 Hz, 2H), 3.43 (m, 1H), 2.64 (m, 1H), 2.44 (m, 1H), 2.29 (m, 2H) 2.17 (m, 1H), 1.78-1.56 (m, 6H), 1.32 (m, 2H), 1.21 (m, 2H), 1.07 (m, 2H). ¹³C-NMR (125 MHz, CD₃OD) δ 209.7, 173.7, 147.8, 137.8, 73.6, 70.0, 64.8, 62.2, 40.3, 39.9, 39.0, 36.9, 33.7, 33.3, 27.5, 27.01, 26.6 (×2). HRFABMS *m/z* 325.2011 [M+H]⁺ (calcd for C₁₈H₂₈O₅, 325.2010).

5.1.15. 2-(2-Methoxyethoxy)ethyl-2-(2-(cyclohexylmethylene)-3-oxocyclopentyl)acetate

(E/Z)-5i

Yellow oil; 54% yield; ¹H-NMR (500 MHz, CD₃OD) δ 6.40 (dd, *J* = 10.7, 1.7 Hz, 1H), 4.29 (m, 2H), 3.73 (m, 2H), 3.68 (m, 2H), 3.59 (m, 2H), 3.51 (m, 1H), 3.40 (s, 3H), 2.60 (m, 2H), 2.49 (m, 1H) 2.34 (m, 2H), 2.09 (m, 1H), 1.96 (m, 1H), 1.80 (m, 2H), 1.69 (m, 2H), 1.40 (m, 2H), 1.27 (m, 4H). ¹³C-NMR (125 MHz, CD₃OD) δ 209.2, 173.4, 143.7, 139.5, 72.9, 71.3, 70.0, 64.7, 59.1, 40.2, 39.6, 36.6, 36.2, 33.1, 33.0, 26.8, 26.4, 26.3 (×2). HRFABMS *m/z* 339.2166 [M+H]⁺ (calcd for C₁₉H₃₀O₅, 339.2166).

5.1.16. 2-(2-(2-Hydroxyethoxy)ethoxy)ethyl-2-(2-(cyclohexylmethylene)-3-

oxocyclopentyl)acetate (E)-5j

Yellow oil; 56% yield; ¹H-NMR (500 MHz, CD₃OD) δ 6.39 (dd, *J* = 10.7, 1.7 Hz, 1H), 4.29 (t, *J* = 6.8 Hz, 2H), 3.75 (t, *J* = 6.6 Hz, 2H), 3.69 (m, 6H), 3.58 (t, *J* = 6.4 Hz, 2H), 3.50 (m, 1H), 2.57 (m, 2H), 2.50 (m, 1H) 2.34 (m, 2H), 2.09 (m, 1H), 1.95 (m, 1H), 1.79 (m, 2H), 1.69 (m, 2H), 1.42 (m, 2H), 1.27 (m, 4H). ¹³C-NMR (125 MHz, CD₃OD) δ 209.2, 173.4, 143.7, 139.4, 73.6, 71.5, 71.4, 70.0, 64.7, 62.2, 40.2, 39.6, 36.6, 36.2, 33.1, 33.0, 26.8, 26.4, 26.3 (×2). HRFABMS *m/z* 369.2273 [M+H]⁺ (calcd for C₂₀H₃₂O₆, 369.2272).

5.1.17. 2-(2-(2-Hydroxyethoxy)ethoxy)ethyl-2-(2-(cyclohexylmethylene)-3-

oxocyclopentyl)acetate (Z)-5j

Yellow oil; 8% yield; ¹H-NMR (500 MHz, CD₃OD) δ 5.83 (dd, *J* = 9.6, 2.0 Hz, 1H), 4.29 (t, *J*

= 6.8 Hz, 2H), 3.73 (t, $J = 6.6$ Hz, 2H), 3.67 (m, 6H), 3.58 (t, $J = 6.4$ Hz, 2H), 3.45 (m, 1H), 2.67 (m, 1H), 2.45 (m, 1H) 2.33 (m, 2H), 2.20 (m, 1H), 1.74 (m, 2H), 1.64 (m, 2H), 1.34 (m, 4H), 1.24 (m, 2H), 1.10 (m, 2H). $^{13}\text{C-NMR}$ (125 MHz, CD_3OD) δ 209.4, 173.7, 147.7, 137.7, 73.7, 71.5, 71.4, 70.1, 64.6, 62.2, 40.2, 39.9, 39.0, 36.9, 33.7, 33.3, 27.5, 27.0, 26.6 ($\times 2$).
 HRFABMS m/z 369.2273 $[\text{M}+\text{H}]^+$ (calcd for $\text{C}_{20}\text{H}_{32}\text{O}_6$, 369.2272).

5.1.18. *2-(2-(2-Methoxyethoxy)ethoxy)ethyl-2-(2-(cyclohexylmethylene)-3-oxocyclopentyl)acetate (E/Z)-5k*

Yellow oil; 30% yield; $^1\text{H-NMR}$ (500 MHz, CD_3OD) δ 6.37 (dd, $J = 10.7, 1.8$ Hz, 1H), 4.25 (m, 2H), 3.71 (m, 2H), 3.65 (m, 6H), 3.56 (m, 2H), 3.45 (m, 1H), 3.37 (s, 3H), 2.54 (m, 2H), 2.47 (m, 1H) 2.31 (m, 2H), 2.06 (m, 1H), 1.92 (m, 1H), 1.78 (m, 2H), 1.66 (m, 2H), 1.39 (m, 2H), 1.25 (m, 4H). $^{13}\text{C-NMR}$ (125 MHz, CD_3OD) δ 209.2, 173.4, 143.7, 139.5, 72.9, 71.5, 71.5, 71.3, 70.0, 64.8, 59.1, 40.2, 39.6, 36.6, 36.2, 33.1, 33.0, 26.8, 26.4, 26.3, 26.3 ($\times 2$).
 HRFABMS m/z 405.2247 $[\text{M}+\text{H}]^+$ (calcd for $\text{C}_{21}\text{H}_{34}\text{O}_6$, 405.2248).

5.1.19. *2-Hydroxypropyl-2-(2-(cyclohexylmethylene)-3-oxocyclopentyl)acetate (E/Z)-5l*

Yellow oil; 64% yield; $^1\text{H-NMR}$ (500 MHz, CD_3OD) δ 6.38 (dd, $J = 10.7, 1.7$ Hz, 1H), 4.05 (m, 1H), 3.99 (m, 2H), 3.50 (m, 1H), 2.57 (m, 2H), 2.49 (m, 1H) 2.33 (m, 2H), 2.07 (m, 1H), 1.93 (m, 1H), 1.79 (m, 2H), 1.66 (m, 2H), 1.38 (m, 2H), 1.30 (m, 4H), 1.21 (d, $J = 1.9$ Hz, 3H). $^{13}\text{C-NMR}$ (125 MHz, CD_3OD) δ 209.3, 173.4, 143.7, 139.5, 70.4, 66.3, 40.2, 39.6, 36.6, 36.2, 33.1, 33.0, 26.8, 26.4 ($\times 2$), 26.3, 19.6. HRFABMS m/z 295.1904 $[\text{M}+\text{H}]^+$ (calcd for $\text{C}_{17}\text{H}_{26}\text{O}_4$, 295.1904).

5.1.20. *Synthesis of compounds 7a-7b*

Acyl chloride **6**, which was prepared by reaction of acid **4** with an excess amount of oxalyl chloride in dichloromethane at 45°C for 1 h, was treated with isopropylamine and *N*-methylethanolamine in the presence of TEA (1 equiv), *N,N*-dicyclohexylcarbodiimide (DCC) (0.1 equiv), 1-hydroxybenzotriazole (HOBT) (0.1 equiv) in dichloromethane at room temperature for 12 h to yield the intermediate esters **7a-7b**. The mixture was washed with water, dried, concentrated to give a residue and was then purified by reversed-phase HPLC (YMC ODS-Triart C18 column) to yield the target amides **7a-7b**.

5.1.21. 2-(2-(Cyclohexylmethylene)-3-oxocyclopentyl)-N-isopropylacetamide (E/Z)-7a

Yellow oil; 55% yield; ¹H-NMR (500 MHz, CD₃OD) δ 6.44 (dd, *J* = 10.7, 1.8 Hz, 1H), 3.99 (m, 1H), 3.52 (m, 1H), 2.67 (m, 1H), 2.44 (m, 1H), 2.26 (m, 1H), 2.07 (m, 1H), 1.77 (m, 3H), 1.70 (m, 4H), 1.38 (m, 3H), 1.25 (m, 4H), 1.16 (d, *J* = 6.6 Hz, 3H), 1.12 (d, *J* = 6.6 Hz, 3H). ¹³C-NMR (125 MHz, CD₃OD) δ 197.1, 172.5, 144.7, 141.9, 43.3, 39.9, 34.0, 33.2 (×2), 32.5, 26.8, 26.5, 26.4, 25.1 (×2), 22.8 (×2). HRFABMS *m/z* 278.2115 [M+H]⁺ (calcd for C₁₇H₂₇NO₂, 278.2115).

5.1.22. 2-(2-(Cyclohexylmethylene)-3-oxocyclopentyl)-N-(2-hydroxyethyl)-N-methylacetamide (E/Z)-7b

Yellow oil; 56% yield; ¹H-NMR (500 MHz, CD₃OD) δ 6.36 (dd, *J* = 10.9, 1.8 Hz, 1H), 3.71 (m, 2H), 3.56 (m, 2H), 3.50 (m, 1H), 3.00 (s, 3H), 2.75 (m, 1H), 2.54 (m, 1H), 2.48 (m, 1H), 2.29 (m, 2H), 2.02 (m, 1H), 1.89 (m, 1H), 1.79 (m, 2H), 1.67 (m, 2H), 1.39 (m, 2H), 1.25 (m, 4H). ¹³C-NMR (125 MHz, CD₃OD) δ 209.9, 174.3, 143.3, 140.5, 60.1, 53.1, 39.6, 39.0, 37.6, 36.7, 36.5, 34.0, 33.1 (×2), 26.8, 26.4 (×2). HRFABMS *m/z* 294.2061 [M+H]⁺ (calcd for C₁₇H₂₇NO₃, 294.2064).

*5.2. Biological methods**5.2.1. Cell culture and cell viability*

RAW264.7 murine macrophages were purchased from the Korean Cell Line Bank (KCLB®, Seoul, Korea). Rat liver Ac2F cells were obtained from the American Type Culture Collection (ATCC, Rockville, MD, USA). Cells were cultured at 37°C in a 5% CO₂ humidified incubator and maintained in high glucose Dulbecco's Modified Eagle Medium (DMEM, Nissui, Tokyo, Japan) containing 100 mg/mL streptomycin, 2.5 mg/L amphotericin B, and 10% heat-inactivated fetal bovine serum (FBS). Suspensions of tested cell lines (cal. 1.0 × 10⁴ cells/well) were seeded in a 96-well culture plates and cultured for 12 h followed by treatment with various diluted concentrations of test compounds for 24 h. Control cultures were treated with culture medium alone. The tested compounds were evaluated at two dilutions and the highest concentration was 50 μM. Cell viabilities were evaluated using a

water soluble tetrazolium (WST) reagent (EZ-CyTox, Daeil Lab Service Co., Ltd., Seoul, Korea), which was added to each well (10 μ L) and incubated at 37°C for 1 h. Absorbances were read using an iMark Microplate Absorbance Reader (Bio-Rad Laboratories, Hercules, CA, USA) at a wavelength of 450 nm. Cells in the exponential phase were used for all experiments.

5.2.2. *Luciferase assay*

Rat liver Ac2F cells were obtained from the American Type Culture Collection (ATCC, Rockville, MD, USA). Cells were grown in Dulbecco's Modified Eagle Medium (DMEM, Nissui, Tokyo) containing 2 mM L-glutamine, 100 mg/mL streptomycin, 2.5 mg/L amphotericin B and 10% fetal bovine serum (FBS) and maintained in a humidified atmosphere containing 5% CO₂ at 37°C. The TK-PPRE \times 3-luciferase reporter plasmid, containing 3 copies of the PPRE in the acyl CoA oxidase promoter was generously donated by Dr. Christopher K. Glass (University of California at San Diego, La Jolla, CA, USA). The pcDNA3 expression vector and full-length human PPAR γ 1 expression vector (pFlag-PPAR γ 1) were generously donated by Dr. Chatterjee (the University of Cambridge, Addenbrooke's Hospital at Cambridge, UK). The Lipofectamine™ 2000 transfection reagent was generously donated by Invitrogen Co. (Carlsbad, CA, USA). For the luciferase assays, proper plasmids were transfected into Ac2F cells in a 48-well plate (5×10^4 cells/well) with effector plasmids, and TK-PPRE \times 3-luciferase reporter plasmid, pcDNA3, and pFlag-PPAR γ 1 using Lipofectamine™ 2000 according to the manufacturer's instructions. After transfection for 4 h, the conditioned media was removed and replaced with complete media, and the cells were incubated for an additional 20 h. The medium was then removed, and cells were exposed in serum-free media to rosiglitazone or test compounds for 6 h. Washed with PBS and assayed using Steady-Glo Luciferase Assay System (Promega, Madison, WI, USA). Luciferase activity was measured using a GloMax-Multi Microplate Multimode Reader (Promega Corporation, CA, USA).

5.2.3. *In vitro stability assessment assay*

The mixture of the synthesized compounds (0.5 mg) and 50 μ L of porcine liver esterase (Sigma Chemical; Lot no. E2884-1KU: 1000U/0.34MI; 1 unit (1U) of the enzyme hydrolyzes 1 μ mol of an ester) in 0.01 M phosphate buffer solution (pH 7.4, 1 mL) and acetone (12 μ L) was incubated at 37°C. At regular intervals (30 and 60 min), the reacted products (500 μ L) were withdraw and directly injected into Shimadzu LC-20A HPLC with a YMC ODS-Triart C18 column (250 \times 10 mm, 5 μ m, 120 Å) for analysis using 5-95% gradient MeOH as the mobile phase, with a flow rate of 1 mL/min, and the UV detection at 210 and 254 nm. The ratio of intact esters/amides and their corresponding acids were analyzed by calculating the areas size.

5.2.4. *Production levels of NO and cytokines released into the medium*

RAW264.7 macrophages (cal. 1×10^4 cells/well) were seeded in a 96-well culture plate and cultured for 12 h. Cells were pre-treated with various concentrations of the drugs for 1 h and then co-incubated with 25 ng/mL of LPS for 24 h. NO concentrations in the medium were determined using Griess assay. Griess reagent (80 μ L) was added to the media supernatants (80 μ L) and then incubated at 37°C for 15 min in the dark. Absorbance was measured at 520 nm using an iMark Microplate Absorbance Reader (Bio-Rad Laboratories, Hercules, CA, USA). NO concentrations were calculated using 0-100 μ M sodium nitrite standards. TNF- α and IL-6 expression levels in culture medium were quantified using a sandwich-type ELISA kit (Biolegend, San Diego, CA, USA). Absorbance was measured at 450 nm.

5.2.5. *Immunofluorescence staining of NF- κ B p65 in RAW264.7 cells*

Cells were grown on a confocal dish and treated with the compound for 24 h and then co-incubated with 1 μ g/mL of LPS for 30 min. Cells were then fixed in 10% formalin solution for 15 min, washed thrice with PBS, treated with 0.5% (v/v) Triton X-100/PBS for 15 min, washed thrice with PBS, and then blocked at room temperature for 30 min in 10% FBS/PBS. Cells were then incubated with rabbit anti-NF κ B-p65 antibody (Cell signaling technology, USA) at 4°C overnight, washed thrice with PBS, incubated for 30 min at room temperature with secondary antibody anti-rabbit Alexa 488 (Cell signaling technology, USA) as the

molecular probe, washed thrice with PBS, and then incubated with PI/Rnase (10 µg/mL) at room temperature for 20 min. The location of NFκB-p65 was determined by confocal microscopy FluoView FV10i (Olympus, Australia) using an excitation wavelength of 488 nm and an emission wavelength of 537 nm.

5.2.6. *Western blot assay*

RAW264.7 cells were harvested and suspended in lysis buffer containing protease and phosphatase inhibitor cocktails. Protein concentrations were determined using a BCA protein assay (Thermo Scientific, Rockford, IL, USA). Equal amounts of protein were resolved by 10% SDS-polyacrylamide gel electrophoresis and were electrophoretically transferred to polyvinylidene difluoride (PVDF) membranes; these were then blocked in Tris-buffered saline containing 0.1% Tween 20 (TBS-T) and 5% skimmed milk for 1 h at room temperature, and then incubated with specific primary antibodies (Cell Signaling Technology, Danvers, MA, USA) overnight at 4°C. Anti-rabbit IgG-HRP was used as the secondary antibody. Signals were developed using the ChemiDoc™ Touch Imaging System (Bio-Rad Laboratories, Hercules, CA, USA).

5.2.7. *Reactive oxygen species (ROS) measurement*

RAW264.7 macrophages were grown on a confocal dish and treated with the test compound for 1 h. LPS solution was added into the dish at a final concentration of 1 µg/mL and continually cultured for 24 h. The medium was removed and washed with PBS; DCFH-DA diluted in FBS-free medium to a final concentration of 100 µM was added and cultured at 37°C for 30 min. The medium was removed and the cells were washed once with PBS. The fluorescence was observed using a confocal microscope (FluoView FV10i; Olympus, Australia) with an excitation wavelength of 485 nm and an emission wavelength of 520 nm.

Quantification of cellular oxidative stress was performed by using a previously reported method [30,31]. RAW264.7 macrophages (cal. 1×10^4 cells/well) were seeded into black 96-well cell culture plates and cultured for 12 h. The cells were pre-treated with the test compound for 1 h and then co-incubated with 1 µg/mL LPS for 24 h. The medium was removed and washed with PBS; 100 µL DCFH-DA diluted in FBS-free medium to a final

concentration of 100 μM was added and cultured at 37°C for 30 min. The medium was then removed, 100 μL PBS was added to each well, and fluorescence was detected at an excitation wavelength of 485 nm and an emission wavelength of 520 nm using the TriStar LB 941 Multimode Microplate Reader (Bad Wildbad, Germany).

5.2.8. *Statistical analysis*

The significance of intergroup differences was determined by one-way analysis of variance (ANOVA) using SPSS 13.0. Results are expressed as the mean \pm SD of the indicated numbers of independent experiments. Values of $p < 0.05$ were considered statistically significant.

5.2.9. *Molecular Modeling*

Docking calculations were performed using Auto Dock Vina 1.1.2 software. The default settings and scoring function of Vina were applied. The AMBER force field was applied for energy minimization. For ligand preparation, Chem3D Ultra 8.0 software was used to convert the 2D structures of the candidates into 3D structural data and to prepare the chemical structures with minimized energy. Protein coordinates were downloaded from the Protein Data Bank (accession code 2PRG). Chain A was prepared for docking within the molecular modeling software package, Chimera 1.5.3, by removing chain B and all ligands and water molecules (except water molecules 308, 399, 444, and 467), and by calculating the protonation state of the protein. Addition of polar hydrogen and setting of grid box parameters was performed using MGLTools 1.5.4. PyMol v1.5 was used to analyze and visually investigate the ligand-protein interactions of the docking poses.

Disclosure statement

No potential conflict of interest was reported by the authors.

Funding

This research was supported by the National Research Foundation of Korea (NRF 201901920001). M. Su was supported by the PNU postdoc program (2018), and Z.R. Ju was partially supported by China Scholarship Council (No. 201608260116).

References

- [1] L.M. Coussens, Z. Werb, Inflammation and cancer, *Nature* 420 (2002) 860.
- [2] C.A. Feghali, T.M. Wright, Cytokines in acute and chronic inflammation, *Front. Biosci.* 2 (1997) d12-d26.
- [3] A. Mantovani, C. Garlanda, P. Allavena, Molecular pathways and targets in cancer-related inflammation, *Ann. Med.* 42 (2010) 161-170.
- [4] M. Park, J. Hong, Roles of NF- κ B in cancer and inflammatory diseases and their therapeutic approaches, *Cells*, 5 (2016) 15.
- [5] S.A. Kliewer, H.E. Xu, M.H. Lambert, T.M. Willson, Peroxisome proliferator-activated receptors: From genes to physiology, *Recent. Prog. Horm. Res.* 56 (2001) 239-263.
- [6] B.M. Spiegelman, PPAR- γ : adipogenic regulator and thiazolidinedione receptor, *Diabetes* 47 (1998) 507-514.
- [7] M. Ricote, A.C. Li, T.M. Willson, C.J. Kelly, C.K. Glass, The peroxisome proliferator-activated receptor- γ is a negative regulator of macrophage activation, *Nature* 391 (1998) 79.
- [8] G.J. Murphy, J.C. Holder, PPAR- γ agonists: therapeutic role in diabetes, inflammation and cancer, *Trends. Pharmacol. Sci.* 21 (2000) 469-474.
- [9] Z.R. Ju, M.Z. Su, J.K. Hong, S. Ullah, E.L. Kim, C.H. Zhao, H.R. Moon, S.M. Kim, J.H. Jung, Design of PPAR- γ agonist based on algal metabolites and the endogenous ligand 15-deoxy- $\Delta^{12,14}$ -prostaglandin J₂, *Eur. J. Med. Chem.* 157 (2018) 1192-1201.
- [10] Z.R. Ju, M.Z. Su, D.D. Li, J.K. Hong, D.S. Im, S.M. Kim, E.L. Kim, J.H. Jung, An Algal Metabolite-Based PPAR- γ Agonist Displayed Anti-Inflammatory Effect via Inhibition of the NF- κ B Pathway, *Mar. Drugs.* 17 (2019) 321.

- [11] T. Shiraki, N. Kamiya, S. Shiki, T.S. Kodama, A. Kakizuka, H. Jingami, α , β -unsaturated ketone is a core moiety of natural ligands for covalent binding to peroxisome proliferator-activated receptor γ , *J. Biol. Chem.* 280 (2005) 14145-14153.
- [12] T. Waku, T. Shiraki, T. Oyama, K. Morikawa, Atomic structure of mutant PPAR γ LBD complexed with 15dPGJ₂: Novel modulation mechanism of PPAR γ /RXR α function by covalently bound ligands, *FEBS Lett.* 583 (2009) 320-324.
- [13] C. Chapuis, G.H. Büchi, H. Wüest, Synthesis of *cis*-Hedione and Methyl Jasmonate via Cascade *Baylis–Hillman* Reaction and *Claisen* Ortho Ester Rearrangement, *Helv. Chim. Acta.* 88 (2005) 3069-3088.
- [14] M.H. Saied, R. Gatri, A.S. Al-Ayed, Y. Arfaoui, M.M.E Gaied, A Short Route to the Ester (\pm) HomoSarkomycin via Johnson-Claisen Rearrangement, *Lett. Org. Chem.* 14 (2017) 181.
- [15] H.T. Dang, Y.M. Lee, G.J. Kang, E.S. Yoo, J.K. Hong, S.M. Lee, S. K. Lee, Y. Pyee, H.J. Chung, H.R. Moon, H.S. Kim, J.H. Jung, In vitro stability and in vivo anti-inflammatory efficacy of synthetic jasmonates, *Bioorg. Med. Chem.* 20 (2012) 4109-4116.
- [16] H.T. Dang, H.J. Lee, E.S. Yoo, J.K. Hong, B.Q. Bao, J.S. Choi, J.H. Jung, New jasmonate analogues as potential anti-inflammatory agents, *Bioorg. Med. Chem.* 16 (2008) 10228-10235.
- [17] K. Sugimoto, M. Yoshida, M. Ihara, Ruthenium-catalyzed ring expansion reaction of 1-acetylenylcyclobutanols with methyl vinyl ketone, *Synlett* 2006 (2006) 1923-1927.
- [18] G. Euglert, M. Vecchi, *trans/cis* Isomerization of Astaxanthin Diacetate/Isolation by HPLC. and Identification by ¹H-NMR. Spectroscopy of Three Mono-*cis*-and Six Di-*cis*-Isomers, *Helv. Chim. Acta.* 63 (1980) 1711-1718.
- [19] K. Eulitz, M.P. Yurawecz, N. Sehat, J. Fritsche, J.A.G. Roach, M.M. Mossoba, J.K.G. Kramer, R.O. Adlof, Y. Ku, Preparation, separation, and confirmation of the eight geometrical *cis/trans* conjugated linoleic acid isomers 8, 10-through 11, 13-18:2, *Lipids* 34 (1999) 873-877.
- [20] R.T. Kroemer, A. Vulpetti, J.J. McDonald, D.C. Rohrer, J.Y. Trosset, F. Giordanetto, S. Cotesta, C. McMartin, M. Kihlén, P.F.W. Stouten, Assessment of docking poses:

- interactions-based accuracy classification (IBAC) versus crystal structure deviations, *J. Chem. Inf. Comput. Sci.* 44 (2004) 871-881.
- [21] O. Trott, A.J. Olson, AutoDock Vina: improving the speed and accuracy of docking with a new scoring function, efficient optimization, and multithreading, *J. Comput. Chem.* 31 (2010) 455-461.
- [22] R.T. Nolte, G.B. Wisely, S. Westin, J.E. Cobb, M.H. Lambert, R. Kurokawa, M.G. Rosenfeld, T.M. Willson, C.K. Glass, M.V. Milburn, Ligand binding and co-activator assembly of the peroxisome proliferator-activated receptor-gamma, *Nature* 395 (1998) 137-143.
- [23] A. Szanto, L. Nagy, The many faces of PPAR γ : anti-inflammatory by any means?, *Immunobiology* 213 (2008) 789-803.
- [24] Y.J. Surh, K.S. Chun, H.H. Cha, S.S. Han, Y.S. Keum, K.K. Park, S.S. Lee, Molecular mechanisms underlying chemopreventive activities of anti-inflammatory phytochemicals: down-regulation of COX-2 and iNOS through suppression of NF- κ B activation, *Mutat. Res.* 480 (2001) 243-268.
- [25] R. Medzhitov, Origin and physiological roles of inflammation, *Nature* 454 (2008) 428.
- [26] S. Cuzzocrea, B. Pisano, L. Dugo, A. Lanaro, P. Maffia, N.S.A. Patel, R.D. Paola, A. Latenti, T. Genovese, P.K. Chatterjee, M.D. Rosa, A.P. Caputi, C. Thiemermann, Rosiglitazone, a ligand of the peroxisome proliferator-activated receptor- γ , reduces acute inflammation. *Eur. J. Pharmacol.* 483 (2004) 79-93.
- [27] M.Z. Su, J.F. Cao, J. Huang, S. Liu, D.S. Im, J.W. Yoo, J.H. Jung, The in vitro and in vivo anti-inflammatory effects of a phthalimide PPAR- γ agonist, *Mar. Drugs.* 15 (2017) 7.
- [28] R. Nemes, E. Koltai, A.W. Taylor, K. Suzuki, F. Gyori, Z. Radak. Reactive oxygen and nitrogen species regulate key metabolic, anabolic, and catabolic pathways in skeletal muscle, *Antioxidants* 7 (2018) 85.
- [29] D.S. Straus, G. Pascual, M. Li, J.S. Welch, M. Ricote, C.H. Hsiang, L.L. Sengchanthalangsy, G. Ghosh, C.K. Glass, 15-Deoxy- $\Delta^{12,14}$ -prostaglandin J₂ inhibits multiple steps in the NF- κ B signaling pathway, *Proc. Natl. Acad. Sci.* 97 (2000) 4844-4849.

- [30] H. Wang, J.A. Joseph, Quantifying cellular oxidative stress by dichlorofluorescein assay using microplate reader, *Free. Radic. Biol. Med.* 27 (1999) 612-616.
- [31] I. Minatel, F. Franciqueti, C. Corrêa, G. Lima, Antioxidant activity of γ -oryzanol: A complex network of interactions, *Int. J. Mol. Sci.* 17 (2016) 1107.

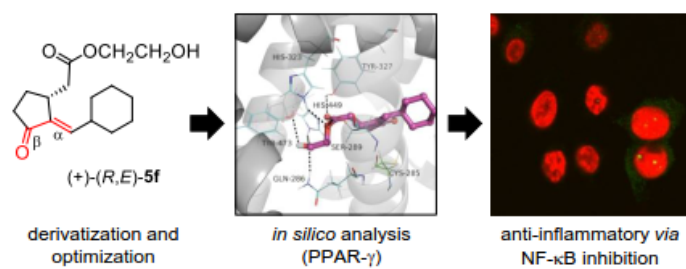
Journal Pre-proofs

Declaration of interests

The authors declare that they have no known competing financial interests or personal relationships that could have appeared to influence the work reported in this paper.

The authors declare the following financial interests/personal relationships which may be considered as potential competing interests:

Journal Pre-proofs



Highlights:

- New PPAR- γ ligands were designed based on (+)-(R,E)-**6a1**.
- Synthetic analogs were evaluated for PPAR- γ activation by luciferase reporter assay.
- Synthetic analogs were evaluated for stability to enzymatic hydrolysis using porcine liver esterase.
- Compound (+)-(R,E)-**5f** showed potent *in vitro* anti-inflammatory activity via inhibition of the NF- κ B pathway.